Deformation driving property of the $h_{9/2}$ configuration in ^{171}Ta

P. Joshi,[1,2] G. Mukherjee,[2] A. Kumar,[1] R. P. Singh,[2] S. Muralithar,[2] S. C. Pancholi,[3] C. R. Praharaj,[4] U. Garg,[5] R. K. Bhowmik,[2] and I. M. Govil[1]

[1]*Department of Physics, Panjab University, Chandigarh 160014, India*

[2]*Nuclear Science Centre, Post Box 10502, New Delhi 110067, India*

[3]*Department of Physics, University of Delhi, Delhi 110021, India*

[4]*Institute of Physics, Bhubaneshwar 751005, India*

[5]*Department of Physics, University of Notre Dame, Notre Dame, Indiana 46556*

(Received 12 October 1998; published 23 August 1999)

The deformation-driving properties of the $h_{9/2}$ configuration in the ^{171}Ta nucleus are discussed in view of the transition probabilities measured for this band. The nucleus of ^{171}Ta was populated using the reaction ^{159}Tb(^{16}O,4n)^{171}Ta at an incident beam energy of 84 MeV. The recoil distance Doppler shift technique was used for the lifetime measurements. The deformation $\beta_2 \sim 0.26$ obtained from these measurements remains almost constant with increasing rotational frequency. The calculated transitional quadrupole moments are compared with the total Routhian surface calculations within the cranked Hartree-Fock-Bogoliubov framework. The measured reduced transition probabilities are compared with those from projected Hartree-Fock microscopic calculations. [S0556-2813(99)08108-X]

PACS number(s): 21.10.Tg, 21.10.Ky, 27.70.+q

I. INTRODUCTION

The deformation-driving properties of the $\pi h_{9/2}$ configuration have been an important point of study in the neutron-deficient Ta isotopes. This configuration comes down sharply in energy for large prolate deformations; hence it is expected to exhibit a strong prolate-driving tendency. The kind of deformation which has been associated with this configuration is almost axially prolate so that changes associated with the γ degree of deformation with increasing rotation are very minimal. Because of the Coriolis decoupling for the low $K(=\frac{1}{2})$ configuration, the maximum alignment of angular momentum occurs right at the onset of the rotation, leaving little room for the changes in the deformation associated with an increase in the alignment of the odd particle.

Because of the minimal changes in the β as well as γ degree of deformation associated with these high j and low K bands, they exhibit a characteristic deformation which can be helpful in studying the configuration dependence of deformation. Their deformation properties, when seen in the context of a particular mass region, may also bring into focus some other correlated aspects of the many-body collective phenomenon, as the observed delayed band crossings of the $h_{9/2}$ band in the tantalum nuclei. The backbending in this band of the Ta isotopes has, in general, been interpreted as the AB band crossings arising due to the alignment of the $i_{13/2}$ neutrons [1–3]. The near-yrast spectroscopic studies of ^{171}Ta [1] have found the AB neutron band crossing to occur at 290 keV for the $h_{9/2}$ proton configuration as compared to 260 keV for bands built on the other configurations, e.g., $[402]\frac{5}{2}^+$, $[404]\frac{7}{2}^+$, and $[514]\frac{9}{2}^-$. The delay in the band crossing $\sim$30 keV for the $h_{9/2}$ band, as compared to the other bands, is interpreted as due to the larger deformation associated with the $h_{9/2}$ configuration in this region. Since lifetime measurements of the $E2$ transitions give concrete and direct information about the quadrupole deformation of the system, therefore such a study would provide a clearer picture of the quadrupole deformations characteristic for this band. We have measured the lifetimes of the members of the $E2$ sequence of the negative parity $h_{9/2}$, $K=\frac{1}{2}$ decoupled band in ^{171}Ta. The results have been compared with the predictions of two important theoretical models, namely, self-consistent cranked Hartree-Fock-Bogoliubov (CHFB) model and the microscopic Hartree-Fock model with angular momentum projections.

II. EXPERIMENTAL DETAILS

Lifetimes were measured using the recoil distance Doppler shift technique [4]. The nucleus ^{171}Ta was populated using the reaction ^{159}Tb(^{16}O,4n)^{171}Ta at a beam energy of 84 MeV, delivered by the 15UD Pelletron at NSC, New Delhi. Three HPGe detectors ($\sim$23% efficiency) were used in the setup along with a 14-element BGO detector array. Two of the HPGe detectors were kept at a backward angle of 144° and one at a forward angle 50° with respect to the beam axis. The 14 element BGO array had 7 elements above and 7 elements below the scattering chamber, looking at the target site. The target used for the experiment was ^{159}Tb (1 mg/cm^2) mounted on a stretcher cone to provide a flat surface. The stopper used was a ^{197}Au (8 mg/cm^2) foil which was sufficient to stop the recoils and was stretched on a similar cone placed exactly opposite to the target foil. The target and stopper distance was calibrated using the capacitance method [5]. The minimum distance was found to be 10 μm from the extrapolation of the distance vs (capacitance)$^{-1}$ plot. A check of the capacitance variation was maintained during the experiment and the distortion of the target-stopper distance, due to the beam falling on it, was found to be less than 1 μm during the experiment.

The NSC Plunger device used for the experiment contains a movable target stretcher cone mounted on three Invar material rods coupled to the axis of three dc linear microactua-

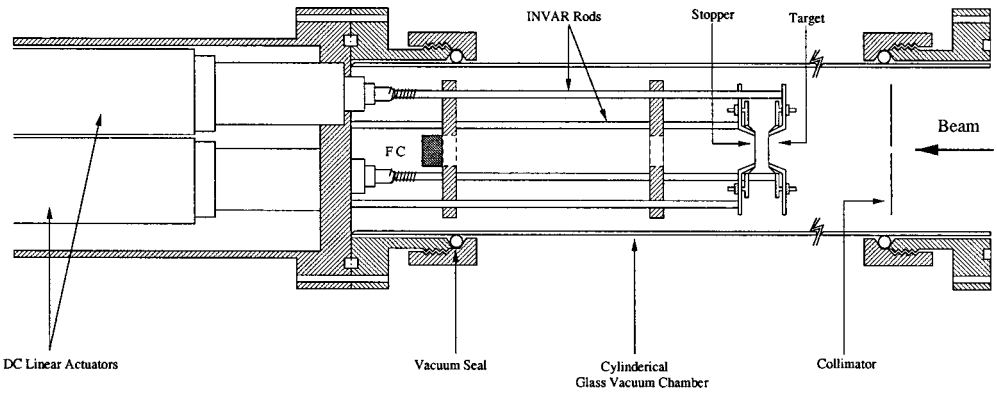

FIG. 1. Schematic of the recoil distance method experimental setup at NSC, used for the experiment.

tors. The stopper cone is mounted on three similar but fixed rods. The target-stopper assembly is aligned with the beam axis and is housed inside a 50 mm diameter glass tube which is used as the scattering chamber, with vacuum couplings on both sides. The experimental setup is shown in Fig. 1. Data were obtained for 17 target-to-stopper distances ($D_{T\text{-}S}$) from 10 to 10 000 μm. The largest distance of 10 000 μm (corresponding to $\tau \sim 3$ ns) ensured that feeding from any long-lived state was properly accounted for. The data were acquired with the hardware condition that at least one of the 14 BGO detectors of the multiplicity filter should fire in coincidence with any of the HPGe detectors. This helped in eliminating contributions due to γ rays from radioactivity and from Coulomb excitation of the target and the stopper. The transitions emanating from levels with spin up to $\frac{25}{2}^-$ in the $h_{9/2}$ band could be seen with their shifted and unshifted partners. The γ rays from higher spins were already shifted at the minimum distance of 10 μm and thus did not qualify as candidates for the measurements using RDM technique.

III. RESULTS AND DISCUSSION

The intensity variations of the shifted and the unshifted peaks for three different D_{T-S} values are shown in Fig. 2. The peaks for shifted as well as the unshifted partners were fitted for different distances. The unshifted intensity data normalized against the total intensity was used for the lifetime analysis, performed with the computer code LIFETIME [6]. This code includes the effect of the unknown side feedings in addition to the known feeding pattern from above. In the case of the topmost level observed, because of the absence of information regarding the levels, the extracted lifetime provides only the upper limit. The minimization and error analysis of the data was done using the package MINUIT [7] used by the program LIFETIME. The errors correspond to the change in the value of the parameter, corresponding to an increment of one unit in χ^2 value on both side of the minimum. Representative decay curves are shown in Fig. 3 and extracted lifetimes and the corresponding $B(E2)$ values are shown in Table I. The measured transition quadrupole moments Q_t and the corresponding deformation β_2 values calculated are plotted in Fig. 4 against the rotational frequency. It is clear from Fig. 4 that there is very little change in the value of Q_t as a function of the rotational frequency. In the case of the $h_{9/2}$ band this constancy of Q_t has been reported for other nuclei (e.g., in ^{177,179}Ir) of this region [8,9].

A. Shape studies using total Routhian surface calculations within CHFB framework

In order to understand the deformation properties of ^{171}Ta, we carried out self-consistent cranked Hartree-Fock-Bogoliubov calculations to find the minima of the potential energy surface so as to predict the shape of the nucleus for the given configuration. In these calculations the single particle energy values were calculated for a Woods-Saxon–type

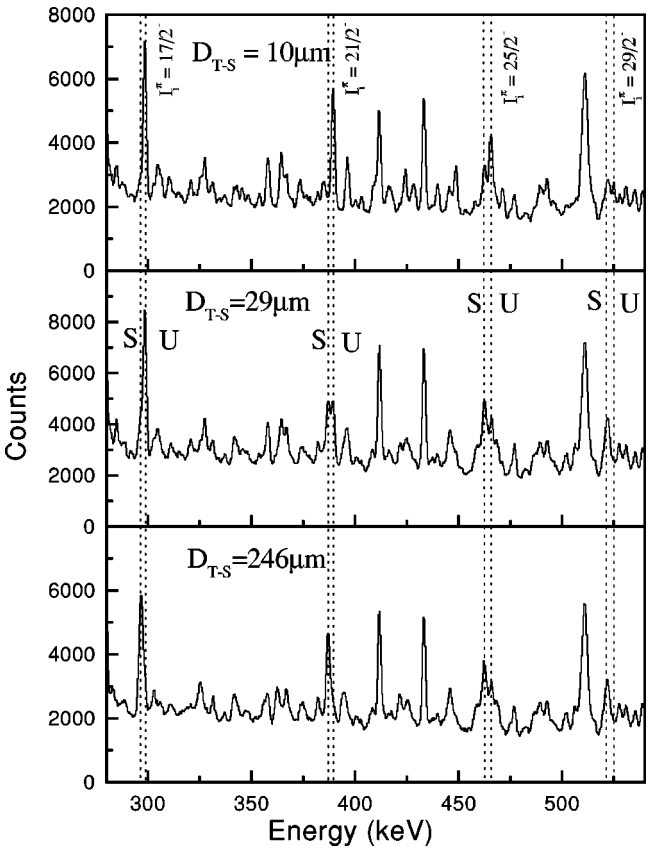

FIG. 2. The shifted (S) and unshifted (U) peaks for transitions in ^{171}Ta for different target to stopper distances ($D_{T\text{-}S}$) at the backward angle (144°).

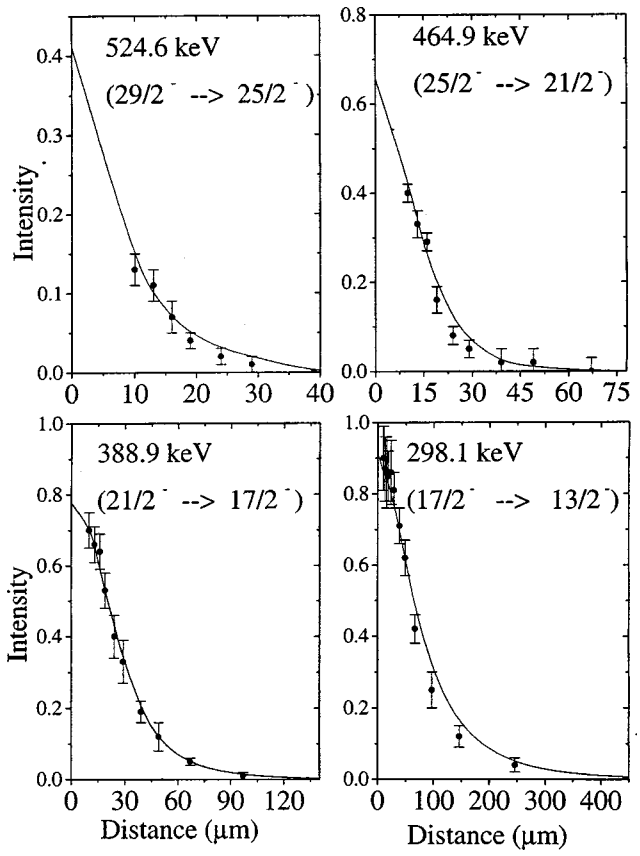

FIG. 3. Decay curves of the normalized unshifted intensities for four different transitions, in the $h_{9/2}$ band of ^{171}Ta.

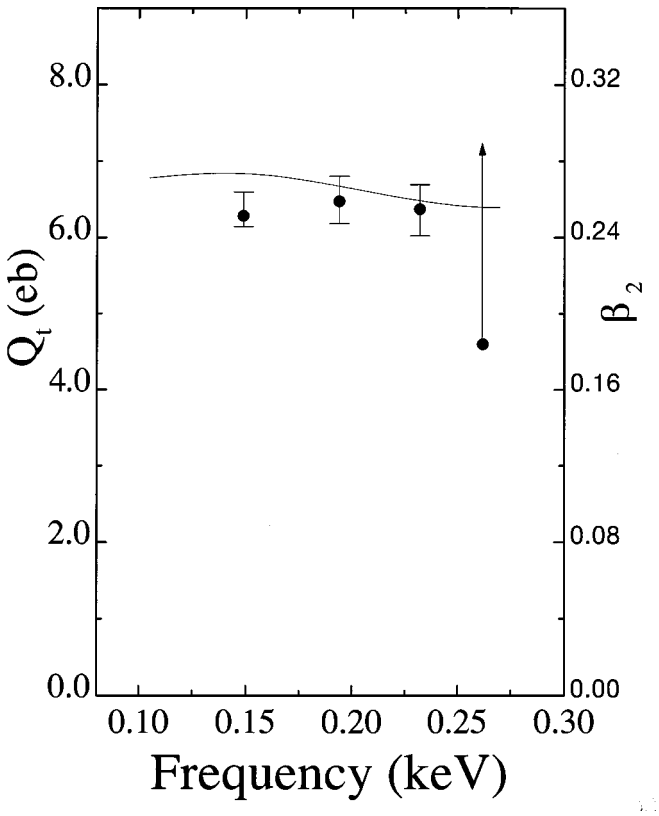

FIG. 4. Experimental values of quadrupole deformations for the $\pi h_{9/2}$ band in ^{171}Ta. The solid curve is the result of cranked shell model calculations.

mean field of quadrupole and hexadecapole deformed shapes [10]. The monopole pairing part of the residual two-body interaction was calculated using the BCS self-consistent procedure [11]. The total cranked Hamiltonian is

$$\hat{H}=\sum_{i_>j_>}[\langle i|\hat{H}_0|j\rangle a_i^\dagger a_j-\omega\langle i|\hat{J}_x|j\rangle a_i^\dagger a_j]-\sum_{i_>j_>}Ga_i^\dagger a_{\bar{i}}^\dagger a_{\bar{j}}a_j, \tag{1}$$

where $\hat{H}_0$ is the single particle Hamiltonian and $a_i^\dagger$ and a_i are the creation and annihilation operators for the particles. The second term is the Coriolis part and the last term is for the residual interaction involving $J=0$ pair coupling. The pairing part is approximated by a one-body pairing potential within the BCS approximation, and the gap parameter Δ and the chemical potential λ are obtained by solving the respective gap and number equations. The pair gap Δ thus calculated was finally used in carrying out the Hartree-Fock-Bogoliubov transformations [12]. The Strutinsky-shell-corrected [13] single particle energies were used as input in these transformations. The Routhians thus calculated were used to generate the total Routhian surface (TRS) plot in the β-γ plane for the given configuration. It is important to mention that special care must be taken for fixed configuration calculations due to the possibility of an adiabatic mixing of different configurations of the same parity and signature. The result of these TRS calculations at a rotational frequency of $\hbar\omega=150$ keV, close to one of the measurements, is shown in Fig. 5. This predicts the minima in the potential energy surface at $\beta_2\sim0.26$ which is in close agreement with the experimental value.

TABLE I. Measured lifetimes and the calculated $B(E2)$ values for the $h_{9/2}$ band in ^{171}Ta.

Energy (keV.)	Spin (I_i^π)	Lifetime (ps)	$B(E2)$ ($e^2\,b^2$)	$B(E2)$ (projected Hartree-Fock) ($e^2\,b^2$)
524.6	$\frac{29}{2}^-$	<2.78	>0.734	1.514
464.9	$\frac{25}{2}^-$	$2.68\pm^{0.32}_{0.25}$	$1.40\pm^{0.15}_{0.15}$	1.511
388.9	$\frac{21}{2}^-$	$6.44\pm^{0.62}_{0.61}$	$1.42\pm^{0.15}_{0.13}$	1.497
298.1	$\frac{17}{2}^-$	$26.46\pm^{1.20}_{2.46}$	$1.30\pm^{0.13}_{0.05}$	1.469

B. Angular momentum projection study of rotational bands of ^{171}Ta

Another way to look at the properties of the $h_{9/2}$ band is to compare the reduced transitional probabilities calculated from a microscopic model with the experimental numbers. The microscopic Hartree-Fock model with the total angular momentum projection is a more practical model to be used for this purpose. In these calculations the Hamiltonian consists of a single particle term and residual two-body interactions. A closed shell core of $Z=50$ and $N=82$ is assumed

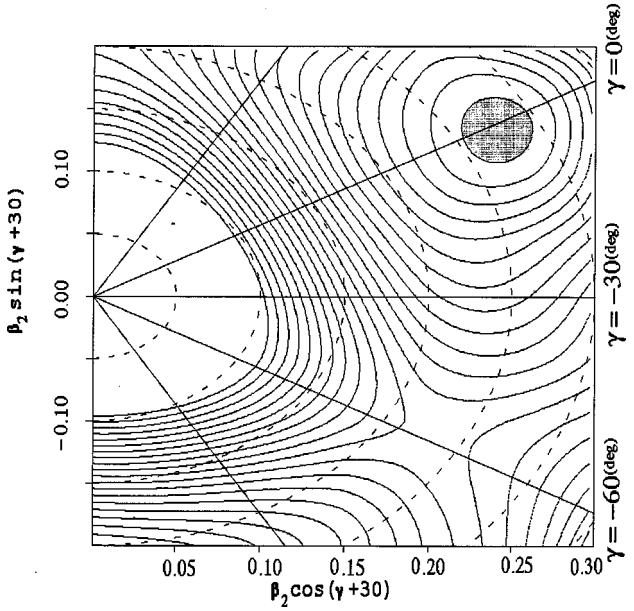

FIG. 5. TRS plot for +ve signature, $\pi h_{9/2}$ configuration for ^{171}Ta at a rotational frequency of 150 keV. Spacing between successive contours is 200 keV.

with one major shell active each for protons and neutrons. A surface delta residual interaction [14], which is known to give reasonable deformation properties of rare-earth nuclei, of strength 0.3 MeV for pp, pn, and nn interactions is used. Axial as well as reflection symmetry of the deformed field [15] is assumed, so that configuration mixing occurs among states of same m values and parity π. Each deformed orbit is denoted by the quantum numbers m^{π}. The prolate deformed Hartree-Fock orbits for protons and neutrons are plotted in Fig. 6. By occupying the lowest proton and neutron orbits and putting the last proton in $m=\frac{1}{2}^-,\frac{9}{2}^-,\frac{5}{2}^+$ near the proton Fermi surface, we generate the band heads for $K=\frac{1}{2}^-,\frac{9}{2}^-,\frac{5}{2}^+$ bands, respectively. It is to be noted that the $m=\frac{1}{2}^-$ orbit occupied by the lone last proton in the $K=\frac{1}{2}^-$ orbit is predominantly of $h_{9/2}$ character.

A given deformed intrinsic state such as any of the bands mentioned above is a superposition of various angular momentum states:

$$|\Phi_K\rangle=\sum_J C_J|\Psi_{JK}\rangle. \tag{2}$$

To get states of definite angular momenta from an intrinsic state we use the angular momentum projection operator

$$\hat{P}^{JM}_K=\frac{2J+1}{8\pi^2}\int D^{J\star}_{MK}(\Omega)\hat{R}(\Omega)d\Omega. \tag{3}$$

Here Ω stands for the Euler angles $(\alpha_1,\theta,\alpha_2)$ and $R(\Omega)$ is the rotation operator:

$$\hat{R}(\Omega)=e^{-i\alpha_1\hat{J}_Z}e^{-i\theta\hat{J}_y}e^{-i\alpha_2\hat{J}_z}. \tag{4}$$

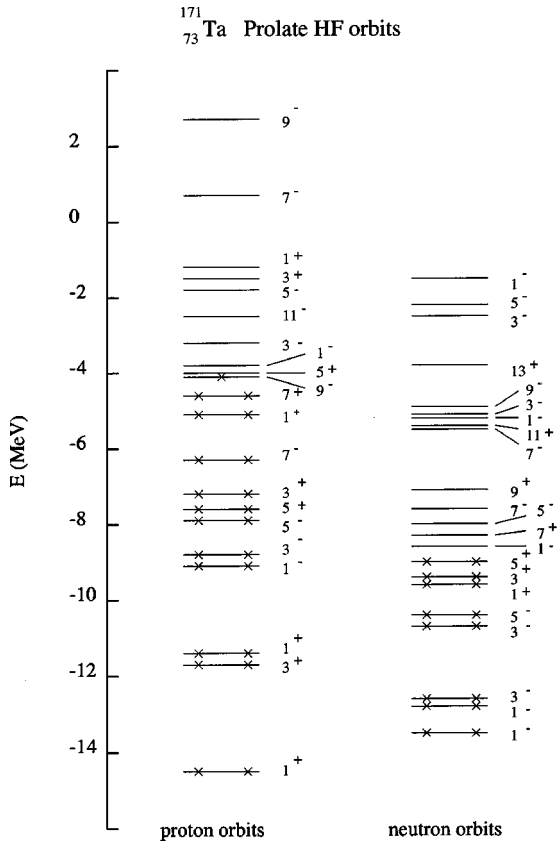

FIG. 6. The prolate deformed Hartree-Fock orbits for protons and neutrons.

For axial symmetry we have the Hamiltonian and wave function overlaps

$$\langle\Psi^{JM}_{K_2}|\hat{H}|\Psi^{JM}_{K_1}\rangle=\frac{2J+1}{2\sqrt{N^J_{K_1K_1}N^J_{K_2K_2}}}\int_0^{\pi}d\theta\sin\theta d^J_{K_2K_1}(J)(\theta)\times\langle\Phi_{K_2}|e^{-i\theta\hat{J}_y}|\Phi_{K_1}\rangle, \tag{5}$$

$$N^J_{K'K}=\frac{2J+1}{2}\int_0^{\pi}d\theta\sin\theta d^J_{K'K}(\theta)\langle\Phi_{K'}|e^{-i\theta\hat{J}_y}|\Phi_K\rangle. \tag{6}$$

The Hamiltonian and overlap kernels in the above two expressions are evaluated. A 64-point Gauss-Legendre quadrature is used in the present calculations. For a tensor operator $\hat{T}^L$ of rank L we have the reduced matrix element

$$\langle\Psi^{I_2}_{K_2}\|\hat{T}^L\|\Psi^{I_1}_{K_1}\rangle=\frac{1}{2}\frac{(2I_1+1)\sqrt{2I_2+1}}{\sqrt{N^I_{K_1K_1}N^I_{K_2K_2}}}\times\sum_{\nu}C^{I_1LI_2}_{K_2-\nu\nu K_2}\int_0^{\pi}d\theta\sin\theta d^{I_1}_{K_2-\nu K_1}(\theta)\times\langle\Phi_{K_2}|\hat{T}^L_{\nu}e^{-i\theta\hat{J}_y}|\Phi_{K_1}\rangle. \tag{7}$$

The calculated reduced transitional probabilities are shown in the last column of Table I. Effective charges of 1.7e for

protons and $0.7e$ for neutrons are used in the calculations. The calculated $B(E2)$ values are quite good in agreement with the experimental results. In fact the constant behavior of the $B(E2)$ values with spin is also visible here which is indicative of no major interaction with another band in the vicinity so as to keep the deformation sustained as a function of spin.

Thus the experimentally measured deformation is theoretically explained using both the phenomenological as well as microscopic models for the band built on $h_{9/2}$ configuration which has the prolate driving tendency because of being high j and low Ω. The natural question arises as to what happens if the odd particle occupies some other high Ω configuration which is not supposed to be as deformed as this one. The band built on the configuration coming from $\Omega = \frac{9}{2}$ component of $h_{11/2}$ is one such candidate where the results for the transitional quadrupole moment are available with deformation $\beta_2 \sim 0.22$ [16]. Thus the deformation ($\beta_2 = 0.26$) of the $h_{9/2}$ band is higher by $\sim 18\%$ than that of $h_{11/2}$ band. Such an enhancement of the deformation is an indication of the deformation-driving property of the low $\Omega = 1/2$ $h_{9/2}$ configuration. In fact, interestingly a very similar trend is also predicted by the theoretical studies of the configuration-dependent deformation by Nazarewicz *et al.* [17] where again the deformation of the $h_{9/2}[541]^{\frac{1}{2}-}$ configuration has been found to be enhanced by almost similar amount ($\sim 15\%$) as compared to that of the $h_{11/2}[514]^{\frac{9}{2}-}$ configuration for the ^{171}Ta nucleus.

IV. SUMMARY

We have measured lifetimes of higher excited states of the $h_{9/2}$ band in ^{171}Ta using the recoil distance method technique and extracted the transition quadrupole moments and the β_2 deformation values. The measured β_2 value (~ 0.26) is found to be nearly constant as a function of rotational frequency. The theoretical values of β_2 obtained from the TRS calculations agree with the present measurements and indicate a prolate deformation. The $B(E2)$ values were calculated using self-consistent microscopic Hartree-Fock calculations with total angular momentum projection. The calculated values are found to be in good agreement with the experimental results. The deformation for the $h_{9/2}$ band is higher by $\sim 18\%$ than that of the $h_{11/2}$ band and points to the deformation-driving property of the $h_{9/2}$ orbital.

ACKNOWLEDGMENTS

The authors are thankful to the Pelletron crew of Nuclear Science Centre, New Delhi, for providing a high quality beam during the course of this experiment. P.J. is thankful to UGC-India for financial support. The U.S. National Science Foundation is acknowledged for Grant No. INT-9309296 to make the international collaboration possible.

[1] J. C. Bacelar *et al.*, Nucl. Phys. **A442**, 547 (1985).
[2] H. Carlsson *et al.*, Nucl. Phys. **A592**, 89 (1995).
[3] W. Shuxian *et al.*, Z. Phys. A **339**, 417 (1991).
[4] T. K. Alexander, in *Advances in Nuclear Physics*, edited by M. Baranger and E. Vogt (Plenum, New York, 1978), Vol. 10, p. 197.
[5] T. K. Alexander and A. Bell, Nucl. Instrum. Methods **81**, 22 (1970).
[6] J. C. Wells *et al.*, Report No. ORNL/TM-9105, 1985.
[7] F. James and M. Roos, Comput. Phys. Commun. **10**, 343 (1975).
[8] D. Muller *et al.*, Phys. Lett. B **332**, 265 (1994).
[9] R. Bengtsson, Nucl. Phys. **A520**, 201c (1990).
[10] J. Dudek *et al.*, Phys. Rev. C **23**, 920 (1981).
[11] S. G. Nilsson and I. Ragnarsson, *Shapes and Shells in Nuclear Structure* (Cambridge University Press, Cambridge, England, 1995).
[12] R. Bengtsson and J. D. Garrett, in *International Review of Nuclear Physics*, edited by T. England *et al.* (World Scientific, Singapore, 1984), Vol. 2.
[13] T. R. Werner and J. Dudek, At. Data Nucl. Data Tables **50**, 179 (1992).
[14] A. Faessler *et al.*, Phys. Rev. **156**, 1064 (1967).
[15] G. Ripka, in *Advances in Nuclear Physics*, edited by M. Baranger and E. Vogt (Plenum, New York, 1968), Vol. I, p. 183.
[16] R. Dogra *et al.*, Hyperfine Interact. **96**, 223 (1995).
[17] W. Nazarewicz, M. A. Riely, and J. D. Garrett, Nucl. Phys. **A512**, 61 (1990).